JOURNAL OF GEOPHYSICAL RESEARCH, VOL. 103, NO. D24, PAGES 31,523–31,539, DECEMBER 27, 1998

The effect of varying the source spectrum of a gravity wave parameterization in a middle atmosphere general circulation model

E. Manzini

Max Planck Institut für Meteorologie, Hamburg, Germany

N. A. McFarlane

Canadian Centre for Climate Modelling and Analysis, Victoria, British Columbia, Canada

Abstract. Climate simulations of the middle atmosphere circulation with general circulation models are now starting to include parameterizations of the momentum flux deposition due to unresolved gravity wave spectra. A current uncertainty in the application of such parameterizations is the specification of the imposed gravity wave spectrum. The aim of this work is to quantify the effect of varying within a realistic range the source spectrum of a gravity wave parameterization in a general circulation model. Results from two simulations with the gravity wave spectrum launched at two different heights, the surface and the 110-hPa pressure level, respectively, are compared. Noteworthy differences found in the simulated middle atmosphere response include the following (1) The average temperature in the southern winter upper stratosphere is about 40 K warmer in the experiment with the surface as the launching height, virtually eliminating the typical cold polar bias that affects many general circulation models. (2) Stronger easterlies in the subtropical summer mesosphere, again in the experiment with the surface as the launching height. Diagnostics of the parameterized gravity waves indicate that in the experiment with the surface as the launching height, the net zonal momentum flux transported by the gravity waves is negative just above the troposphere at middle latitudes. This negative net momentum flux facilitates the deceleration of the mesospheric winter westerlies. The meridional circulation induced by such deceleration is thereafter responsible for the substantial polar winter warming. In contrast, in summer the negative net momentum flux limits the upper mesospheric deceleration of the easterlies. In the experiment with launching height at 110-hPa, the gravity wave net momentum flux is instead zero by construction at the launching height.

1. Introduction

The momentum flux deposition from a spectrum of upward propagating gravity waves is acknowledged to be responsible for the reversal of the temperature gradient at the mesopause and the formation of the winter warm stratopause [*Andrews et al.,* 1987; *Hitchman et al.,* 1989]. In addition to these local effects, mesospheric gravity wave breaking is know to exert a downward control on the stratospheric temperature distribution [*Haynes et al.,* 1991; *McIntyre,* 1992; *Garcia and Boville,* 1994] and to contribute, together with planetary wave breaking, to the dynamical driving of the residual mean meridional circulation; i.e., the large-scale circulation that transports chemical constituents and aerosols in the middle atmosphere [*Holton et al.,* 1995]. The importance of including this circulation in deriving the impact of changes in the atmospheric composition that occur in the troposphere is a motivation for developing climate general circulation models that include the middle atmosphere. However such models have to be integrated for a long time to address the climate problem and therefore have relatively low horizontal resolution, clearly not enough to resolve the relevant (i.e., small scale high frequency) waves. Therefore it is of interest and still very much a field of experimentation to test comprehensive parameterizations of the effects of unresolved gravity wave spectra.

Parameterizations of the momentum flux deposition from a continuous spectrum of gravity waves have recently been developed in order to account for non-orographic waves [*Fritts and Lu,* 1993; *Medvedev and*

Paper number 98JD02274.
0148-0227/98/98JD-02274$09.00

Klaassen, 1995; *Hines,* 1997a, b]. An uncertainty in the application of such a parameterization is the specification of the source spectrum.

In this work a general circulation model is used to examine the response of the circulation in the middle atmosphere to the variations of a parameterized gravity wave source spectrum that are associated with the change in the launching height of the source spectrum. Two 10-year simulations have been performed with the general circulation model, one with a launching height for the continuous spectrum being close to the tropopause and another with this source spectrum launched at the surface. Within the current knowledge, both options are reasonable although an idealization. The purposes of this experimental design are to quantify the sensitivity of the simulated circulation to two extreme cases of the parameterized gravity wave forcing and to determine a possible range of the model responses for the particular gravity wave parameterization employed. The change in the circulation in the middle atmosphere is first examined by looking at the seasonal evolution of the zonal mean low-frequency response as a concise way to summarize and evaluate the basic behavior of the simulations (section 3).

In addition to analyzing the simulated response from the large-scale circulation, it is also of interest to examine differences in the propagation and dissipation of the parameterized gravity waves in the two simulations. This diagnostic of gravity wave parameters will illustrate the effects of the tropospheric wind on the gravity wave spectrum in the case where the spectrum is launched at the surface, and will elucidate the causes of the changes in the middle atmosphere circulation (section 4). Comparisons with similar gravity wave parameters inferred from observations might also suggest which one of the two spectrum configurations at the tropopause is more realistic.

A preliminary investigation of how stationary planetary waves in the northern hemisphere winter are affected by the imposed changes in the gravity wave source spectrum is reported in section 5. Daily variability and short time fluctuations, sudden stratospheric warmings and transient waves will be addressed in a subsequent paper.

2. Design of the Experiments

The general circulation model used is the middle atmosphere (MA) ECHAM4 model developed at the Max Planck Institute in Hamburg. It is an upward extended version of the ECHAM4 model. Most of the physical parameterizations, particularly those that are relevant mainly for tropospheric processes, and the basic model structure are common to both models. A detailed description of the ECHAM4 model is given by *Roeckner et al.* [1996a, b, and reference therein]. The major differences between the two models include the specification of the vertical coordinate and location of model top (ECHAM4 model, top at 10 hPa; MA/ECHAM4 model, top at 0.01 hPa), the parameterization of the effects of gravity waves, and a few modifications in the radiation scheme and in the representation of the horizontal diffusion. The model structure and parameterizations are summarized in Table 1.

In the MA/ECHAM4 model the gravity wave parameterization consists of two parts, separately representing the effects of the momentum deposition from orographic gravity waves and from a continuous gravity wave spectrum. A modified version of the *McFarlane* [1987] parameterization is used to account for the orographic gravity wave drag and will be described in a subsequent paper. The Doppler spread formulation of *Hines* [1997a, b] is used to parameterize the effects of a continuous spectrum of nonorographic gravity waves (Table 1). The implementation of the Doppler spread parameterization (DSP) in the MA/ECHAM4 model follows *Manzini et al.* [1997], with the exception of the way in which the gravity wave source spectrum is prescribed. Namely, the characteristic horizontal wavenumber, the launching height, and the rms wind speed have been modified in the current model version, as outlined below.

Two 10-year simulations that differ only in how the gravity wave spectrum is prescribed have been performed with the MA/ECHAM4 model. In the first integration (CNTRL) the DSP gravity wave source spectrum is launched at 110 hPa with a constant gravity wave rms wind speed of 1.75 m s^{-1}. This spectrum is isotropic relative to the resolved background wind as simulated in the model. In the second integration (EXP2) the source spectrum is launched at the surface with an isotropic and constant gravity wave rms wind speed of 1.5 m s^{-1}. Both rms values of the wind speed have been chosen on the basis of short (few months) numerical experiments so as to ensure values in the ranges of estimates from available observations in the upper troposphere and lower stratosphere [*Allen and Vincent,* 1995; *Fritts and Nastrom,* 1992].

Both simulations include a latitudinal dependence in the characteristic horizontal wavenumber K^*. This latitudinal dependence has been introduced on the assumption that the ratio of the model grid length to the effective gravity wave horizontal wavelength should vary relatively slowly in latitude. We have taken this into account roughly by choosing:

$$K^* = K_{MIN}[\cos\theta + K_{MIN}/K_{MAX}]^{-1} \qquad (1)$$

where θ is the latitude and K_{MIN} and K_{MAX} are given in Table 1.

For all simulations, the sea surface temperature field is specified following the Atmospheric Model Intercomparison Project monthly mean climatology [*Gates,* 1992], the ozone distribution follows the monthly zonal mean from the chemical model of *Brühl* [1993], and the di-

Table 1. MA/ECHAM4 Model: Structure and Parameterizations

Structure/Process	Description
Prognostic variables	Vorticity, divergence, temperature, logarithm surface pressure, specific humidity, mixing ratio of cloud water and a number of optional tracers. The model is based on the primitive equations.
Discretization	Spherical harmonic basis functions with T30 triangular truncation. Nonlinear terms and parameterized physics on the associated Gaussian grid. Second-order finite difference on a hybrid sigma-pressure coordinate system with 39 vertical layers, from the surface to 0.01 hPa (80 km). The vertical resolution is slowly decreasing with height and is about 2 km in the lower stratosphere. Semi-implicit time stepping scheme with a weak filter. A time step of 900 s is used. The radiation scheme is updated every 2 hours. updated every 2 hours.
Transport	The advection of water components and tracers is calculated by using a semi-Lagrangian transport scheme [*Williamson and Rasch*, 1994].
Radiation	The radiation scheme is adopted from ECMWF [*Fouquart and Bonnel*, 1980; *Morcrette*, 1991], with a few modifications: Voigt line shape correction to take into account Doppler broadening at low pressure, inclusion of additional greenhouse gases and optional aerosols, revised parameterization for the water vapor continuum [*Giorgetta and Wild*, 1995], and optical properties for clouds [*Roeckner*, 1995].
Gravity wave parameterizations	The orographic gravity wave parameterization is based on the formulation of *McFarlane* [1987]. The parameterization of momentum flux deposition due to a continuous spectrum of vertically propagating gravity waves follows *Hines* [1997a, b]. An azimuthally isotropic and constant gravity wave variance is assumed at the launching height. At each grid point, eight azimuths (E, NE, N, NW, W, SW, S, and SE) are considered. The initial vertical wavenumber spectrum is proportional to the vertical wavenumber. The characteristic horizontal wavenumber is assumed to increase poleward ($K_{MIN} = 10^{-5}$ m^{-1} and $K_{MAX} = 10^{-4}$ m^{-1}).
Cumulus convection	Mass flux scheme for penetrative, shallow and midlevel convection [*Tiedke*, 1989], with modified detrainment and closure for penetrative convection [*Nordeng*, 1994]. The scheme considers condensation, evaporation, precipitation formation and convective transport of momentum, heat, specific humidity, cloud water and tracers.
Stratiform clouds	Cloud water mixing ratio prognostic equation following *Sundqvist* [1978] to include fractional cloudiness. Sources/sinks due to condensation, evaporation, precipitation and detrained convective cloud water are considered [*Roeckner et al.*, 1991]. The transport terms include semi-Lagrangian advection and turbulent diffusion.
Surface fluxes and vertical diffusion	Turbulent surface fluxes of momentum, heat, specific humidity, cloud water and tracers according to the bulk transfer relation. Above the surface layer, the eddy diffusion method is applied. The eddy viscosity and eddy diffusivity are parameterized in terms of the turbulent kinetic energy [*Brinkop and Roeckner*, 1995].
Horizontal diffusion	The T30 model uses a ∇^{-10} operator with a 6 hour damping time for the highest wavenumber. The horizontal diffusion is enhanced at high wavenumbers for CFL unstable conditions.
Upper level dissipation	At the model top (for a number of levels), Rayleigh friction either on the total flow or on the zonal waves only is optional. Neither is used in the standard version.

urnal and seasonal cycles are included in the radiative transfer calculation.

In order to compare the simulations with observations, the ECMWF reanalysis data are used up to 50 hPa, the combined analysis data [*Randel*, 1992] from the Climate Prediction Center and the National Centers for Environmental Prediction (denoted as the NCEP data set) from 10 to 1 hPa, as well as in the troposphere. For the monthly mean zonal mean temperature and zonal wind the CIRA(1986) data set is also used [*Fleming et al.*, 1990].

3. Changes in the Zonal Mean Response

3.1. Seasonal Evolution of the Zonal Mean Response

The latitude-time evolution of the zonal mean temperature difference between the middle atmosphere model control version, and the ECMWF reanalysis is plotted at 100 and 50 hPa, in Figure 1. A 30-day running mean, averaged over 10 years for the simulation and 15 years (1979-1993) for the reanalysis, is used to illustrate the low frequency seasonal evolution. Fig-

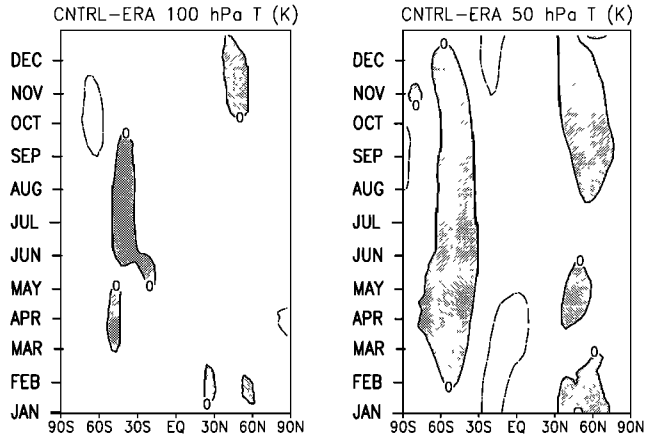

Figure 1. Difference between the CNTRL simulation and the ECMWF reanalysis, CNTRL-ECMWF, for the 30-day running mean of the zonal mean temperature: latitude-time section (left) at 100 hPa and at (right) 50 hPa. The CNTRL temperature is a 10-year ensemble mean. The ECMWF reanalysis temperature is the ensemble mean from a 15-year data set (1979-1993). The contour interval is 5 K (light shading indicates positive values).

ure 1 shows that in the lower stratosphere the zonal mean temperature bias of the control integration with respect to the ECMWF reanalysis is relatively small (less than 5 K) throughout most of the year. Consistently with a small temperature bias, it is found also that the zonal mean low-frequency circulation in the lower stratosphere is realistic, as shown by Figure 2, which depicts the latitude-time evolution of the zonal mean zonal wind at 50 hPa from the reanalysis and the CNTRL experiment. In agreement with the ECMWF reanalysis, in the model control integration it is found that relatively strong westerlies (20-30 m s^{-1}) occur from the beginning of December to the end of January at 60°N, much stronger westerlies occur during the southern hemisphere winter at polar latitudes (above 50 m s^{-1} in August and September); easterlies are found in the summer months (June - July in the northern hemisphere and December - January in the southern), and easterlies are also present in the tropics, stronger at the summer side of the equator. The typical interhemispheric asymmetry in the zonal mean zonal wind strength and in its seasonal evolution (stronger winds at the end the winter in the southern hemisphere versus stronger midwinter winds in the northern hemisphere) in the lower stratosphere is therefore well simulated in this version of the model.

Note that with respect to the ECMWF reanalysis, the zonal mean temperature bias of the control model is quite small (less than 2 K) throughout most of the troposphere while somewhat large (about 10 K) at 200 hPa in the polar regions (not shown). In this respect, the middle atmosphere model is comparable to the ECHAM4 model with top at 10 hPa [*Roeckner et al.*, 1996a].

Although the simulation of the lower stratosphere is quite good in the control simulation, a high-latitude temperature cold bias develops at lower pressure levels during winter, Figure 3. During northern winter the cold bias is still small at 10 hPa, while at 1 hPa it is 10-15 K during November and December, poleward of 60°N. In the southern hemisphere the simulated zonal mean temperature is substantially colder, the largest bias (30-40 K) occurring in July-August at 1 hPa (as for the northern hemisphere, the bias is worse at 1 hPa). Figure 3 also shows that in the southern hemisphere the largest temperature bias occurs later in the season at the lower pressure level (the largest bias is found during September at 10 hPa and during July-August at 1 hPa).

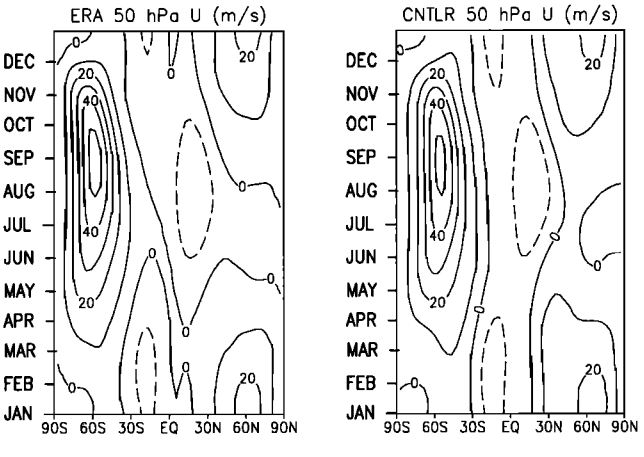

Figure 2. Ensemble mean of the 30-day running mean of the zonal mean zonal wind: (left) from the 15 year ECMWF reanalysis and (right) from the 10-year CNTRL simulation, latitude-time sections at 50 hPa. The contour interval is 10 m s^{-1}.

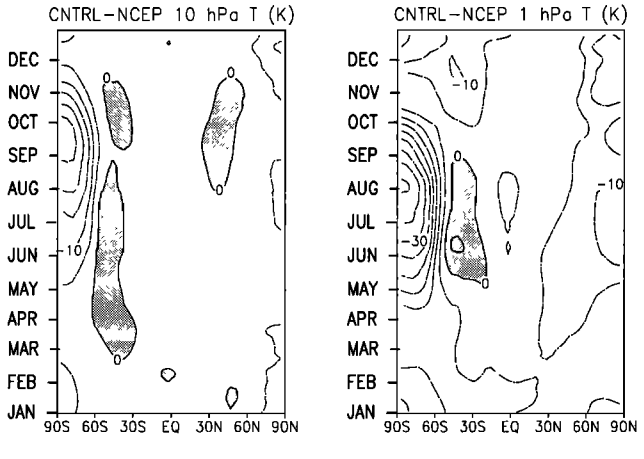

Figure 3. Difference between the CNTRL simulation and the NCEP analysis, CNTRL-NCEP, for the 30-day running mean of the zonal mean temperature: latitude-time section (left) at 10 hPa and (right) at 1 hPa. The CNTRL temperature is a 10-year ensemble mean. The NCEP analysis temperature is the ensemble mean from a 15-year dataset (1979-1993). The contour interval is 5 K (light shading indicates positive values).

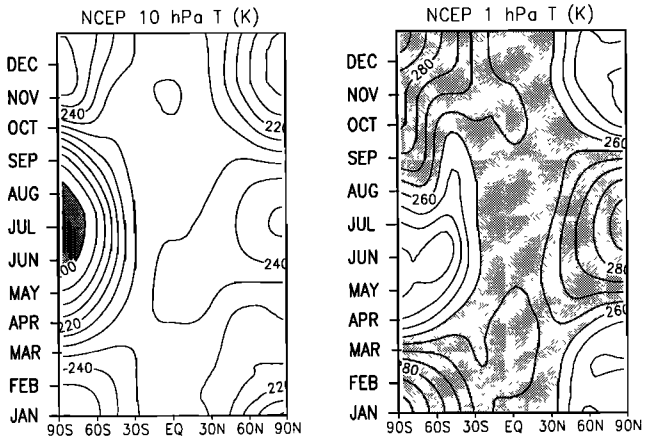

Figure 4. Ensemble mean of the 30-day running mean of the zonal mean temperature from the 15 year NCEP analysis: latitude-time section (left) at 10 hPa and (right) at 1 hPa. The contour interval is 5 K (dark shading, < 200 K; light shading, > 260 K).

At both pressure levels the largest temperature bias in the southern hemisphere seen in Figure 3 therefore occurs during the time of the zonal mean polar temperature increase, i.e., in late winter and early spring after the seasonal temperature minimum (May at 1 hPa and June-July at 10 hPa; see Figure 4). This behavior of the southern hemisphere temperature is in contrast to that of the northern hemisphere, where the largest bias is found in late autumn and early winter. A possible reason for this difference is that planetary wave breaking might play a larger role than gravity wave breaking in the midwinter and spring circulation of the northern hemisphere [*Garcia and Boville,* 1994; *Manzini and Bengtsson,* 1996].

At 1 hPa an additional cold bias is found at polar latitudes in the summer months of both hemispheres. This cold bias might be related to the ozone distribution used or the treatment of the shortwave radiative transfer, although a contribution from the gravity wave parameterization cannot be excluded. Further experiments are needed to clarify this point.

The winter polar temperature bias shown in Figure 3 is expected to be sensitive to the momentum flux deposition from the gravity wave parameterization. General circulation models are in fact known to produce insufficient dynamical driving of the stratospheric circulation from the resolved scales [*Boville,* 1995; *Hamilton et al.,* 1995; *Manzini and Bengtsson,* 1996]. Generally, the meridional temperature field in the middle atmosphere as simulated using a general circulation model with a reasonably comprehensive radiative transfer scheme but no gravity wave parameterization (not even Rayleigh friction on the mean flow) tends toward a temperature field which is significantly different from the observed one and is typical of a radiatively determined temperature field such as that computed by *Fels* [1985] and *Shine* [1987].

In the present context the sensitivity to the variations introduced in the setting of the gravity wave parameterization in the EXP2 integration is illustrated by the change in the temperature bias with respect to the NCEP analysis (Figure 5). In both hemispheres the winter EXP2-NCEP temperature difference is positive at 10 and 1 hPa, indicating a more than successful abatement of the large cold bias present in the control simulation. In fact, the presence of a warm bias suggests too large a role played by the dynamical heating associated with the gravity wave momentum flux deposition, for the EXP2 simulation. At the 1 hPa level the temperature warm bias is particularly large (more than 10 K) in the northern spring (February and March) and in the southern autumn to early winter (April to July). The control simulation was not particularly affected by the cold bias at that level during those periods. The late winter and spring (August to November) temperature bias in the southern hemisphere at 10 hPa is relatively small (5 K), suggesting a realistic breaking down of the polar vortex in the EXP2 integration. Note that the polar summer bias does not appear to be sensitive to the changes in the gravity wave parameterization, supporting other sources of errors, as suggested above. The presence of large and even opposite departures from the observed average state as those seen in Figure 3 and 5 illustrates how difficult it is to obtain absolute improvements in a middle atmosphere general circulation model without introducing spatial and temporal variations in the gravity wave spectrum used in the parameterization.

3.2. Meridional Cross Sections

In this section the sensitivity to the gravity wave parameterization is illustrated for the entire vertical do-

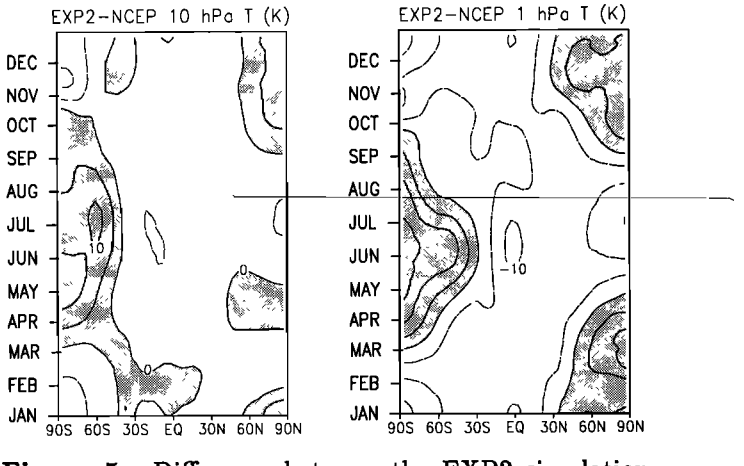

Figure 5. Difference between the EXP2 simulation and the NCEP analysis, EXP2-NCEP, for the 30-day running mean of the zonal mean temperature: latitude-time section (left) at 10 hPa and (right) at 1 hPa. The EXP2 temperature is a 10-year ensemble mean. The NCEP analysis temperature is the ensemble mean from a 15-year dataset (1979-1993). The contour interval is 5 K (light shading indicates positive values).

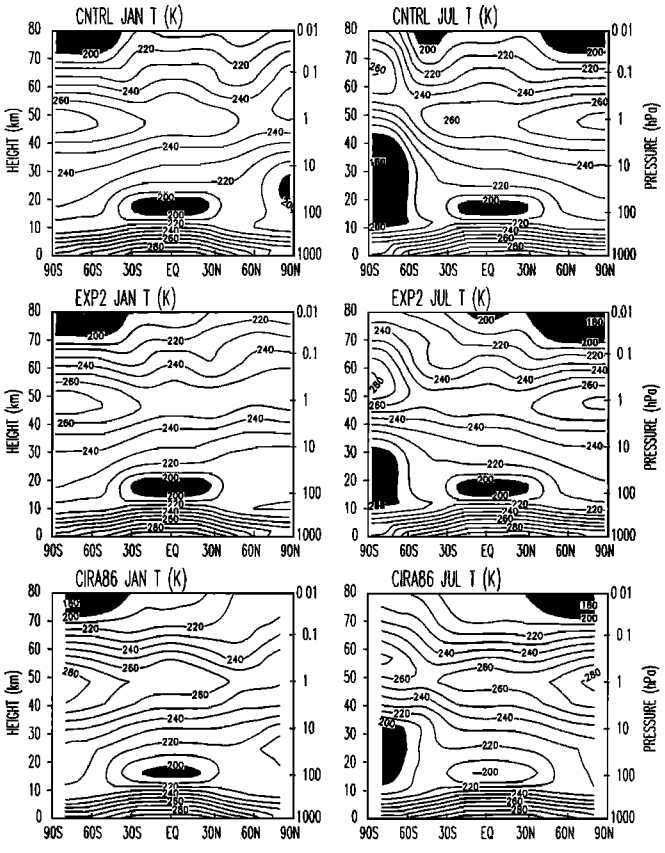

Figure 6. Ensemble mean of the zonal mean temperature (top) from the CNTRL simulation and (middle) from the EXP2 simulation, with (bottom) the CIRA(1986) average. January is at left, and July is at right. The contour interval is 10 K (dark shading indicates < 200 K).

main, focusing on January and July zonal mean fields, 10-year ensemble means. These two months are in fact representative of the most interesting changes occurring between the two simulations. The temperature and zonal wind meridional cross sections are shown in Figures 6 and 7, respectively. In this case the simulations are compared to the CIRA(1986) reference atmosphere [*Fleming et al.*, 1990]. As expected from the latitude-time sections shown previously, Figure 6 indicates remarkable differences between the two model versions for both the northern and southern winters, with the EXP2 simulation generally warmer at polar latitudes in the stratosphere.

In January, the northern polar lower stratosphere temperature of EXP2 is 10-20 K warmer than that of CNTRL. In addition, in January a modest warming is also found poleward of 30°N in the upper mesosphere, bringing the temperature there in closer agreement with the CIRA(1986) data. Note, however, that the CIRA(1986) mesospheric temperatures are based on a limited data set, and may be affected by biases as large as 10 K [*Lawrence and Randel*, 1996; *Lübken and von Zahn*, 1991]. The northern winter polar stratopause in January is less pronounced in experiment EXP2 than in CNTRL.

In the southern winter, large changes in the temperature field between the two experiments are found throughout all the middle atmosphere. The EXP2 warming of the polar stratosphere in July is accompanied by a downward shift of about 10 km of the winter separated stratopause (from 65 km in the control simulation to 55 km in EXP2). The descent of the stratopause in EXP2 is a direct consequence of the circulation changes induced by the parameterized gravity wave driving (see also Figure 8) and is responsible for the occurrence of the largest temperature difference between 50 and 40 km, with the EXP2 simulation more than 40 K warmer at the pole (compare also Figures 3 and 5, at 1 hPa). The comparison of the two simulations with the July CIRA(1986) data indicates that the typical cold bias affecting the CNTRL simulation of the southern hemisphere winter is substantially reduced in EXP2.

Concerning the summer upper mesosphere temperature, a 5 - 10 K cooling is found in July at the North Pole in EXP2 versus control, consistently with a stronger

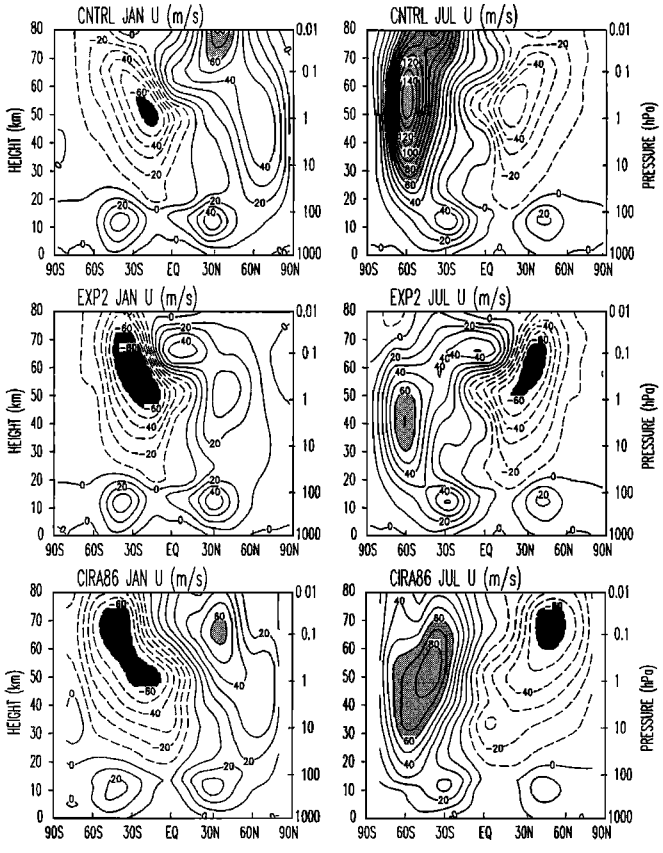

Figure 7. Ensemble mean of the zonal mean zonal wind (top) from the CNTRL simulation and (middle) from the EXP2 simulation, with (bottom) the CIRA(1986) average. January is at left, and July is at right. The contour interval is 10 m s^{-1} (dark shading, < -60 m s^{-1}; light shading, > 60 m s^{-1}).

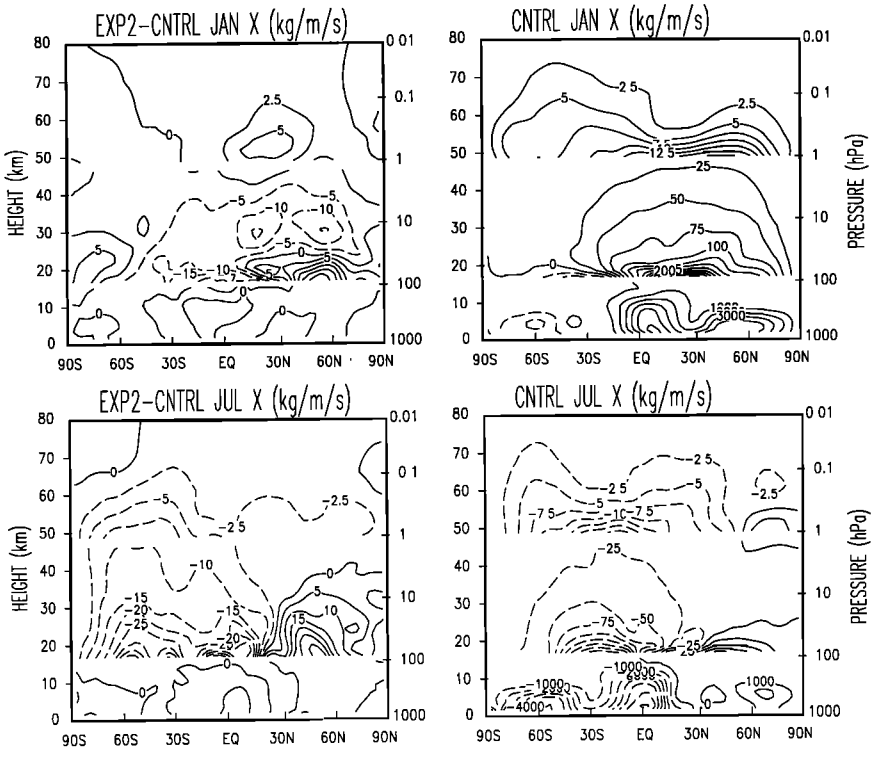

Figure 8. (right) Ensemble mean of the residual mean stream function from the CNTRL simulation and (left) difference between the EXP2 and CNTRL simulations, EXP2-CNTRL, of the ensemble mean of the residual mean stream function. January is at top, and July is at bottom. Contours for the CNTRL fields are 2.5 kg m^{-1} s^{-1} between 0.01 and 1 hPa, 25 kg m^{-1} s^{-1} between 1 and 100 hPa, and 1000 kg m^{-1} s^{-1}, below 100 hPa. Contours for the difference fields are 2.5 kg m^{-1} s^{-1} between 0.01 and 1 hPa, 5 kg m^{-1} s^{-1} between 1 and 100 hPa, and 500 kg m^{-1} s^{-1}, below 100 hPa.

residual circulation (see Figure 8). In January in the summer hemisphere, no significant changes are apparent from Figure 6, but a difference plot (EXP2-CNTRL, not shown) does indicate a cooling of the order of a few degrees. As was found in the previous sections, the summer stratosphere is not much affected in either hemisphere.

Changes in the zonal mean wind are also quite noticeable in the middle atmosphere (Figure 7). In the EXP2 simulation very weak westerlies are found for January in the northern hemisphere, and a single jet of about 30 m s^{-1} and located 1 hPa, 30°N, is present in the middle atmosphere. Concerning the CNTRL experiment, the January winter westerlies are characterized by a more realistic structure, that is, a polar night jet in the lower stratosphere and a subtropical jet in the upper mesosphere. Both CNTRL jets are also of realistic strength (note also that the CIRA(1986) westerlies are weaker than other estimates, eg., *Randel* [1992] and High Resolution Doppler Imager (HARDI) observations [*Fleming et al.*, 1996]). In contrast, in the southern hemisphere, the July polar night jet is more realistic in the EXP2 experiment than in the control integration (also with respect to the other data sets) in the stratosphere, where the EXP2 westerlies are a factor of 2 weaker than that from the CNTRL. However, Figure 7 shows that although the change introduced in the EXP2 version does induce a large reduction in the strength of the July westerlies, it does not help in reproducing the equatorward tilt with height of the jet. Therefore the mesospheric subtropical jet is virtually missing in the EXP2 integration in the southern hemisphere.

At the equator the EXP2 simulation is characterized by a pronounced eastward jet in the middle mesosphere for both January and July. Strong westerlies are also present in the CNTRL at the equator in the mesosphere, a feature related to the semiannual oscillation at the stratopause (i.e., the westward jet seen at 50 km at the equator) that is not substantially different in the two simulations. The dependence of this oscillation on the nonorographic gravity wave parameterization was illustrated by *Manzini et al.* [1997], who used a lower resolution version of the MA/ECHAM4 model. *Manzini et al.* [1997] found that the eastward phase of the oscillation was improved when the DSP parameterization was used (with respect to Rayleigh friction). Comparing the present (CNTRL and EXP2) simulations with each other and with that of *Manzini et al.* [1997], it is found that the semiannual oscillation at the stratopause does not change substantially, supporting the robustness of

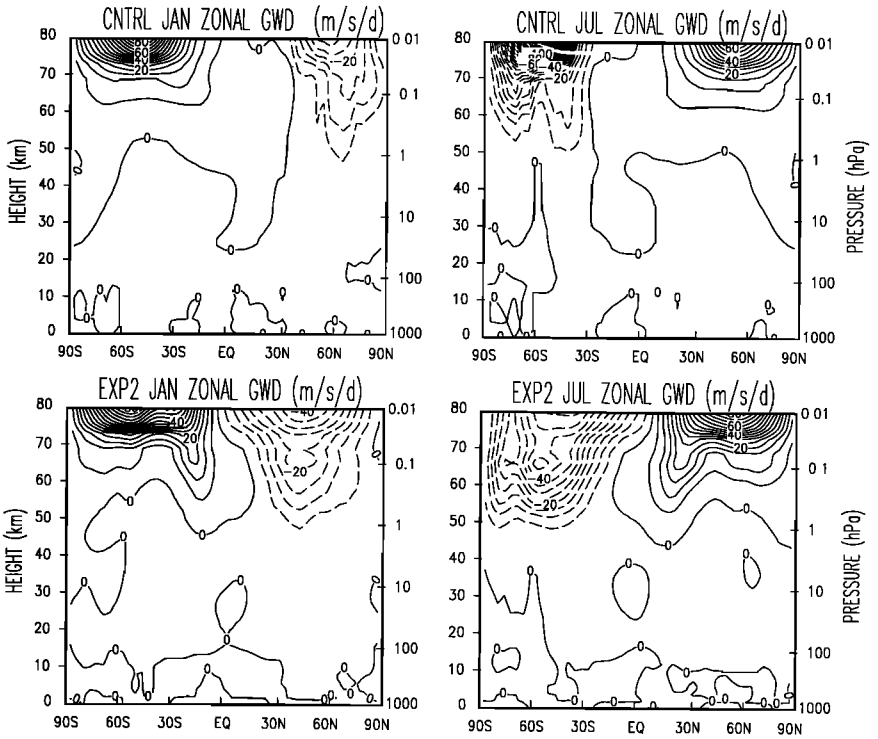

Figure 9. Ensemble mean of the zonal mean of the total (sum of DSP and orographic) gravity wave zonal tendency from (top) the CNTRL and (bottom) the EXP2 simulations. January is at left, and July is at right. The contour interval is 5 m s^{-1} d^{-1}.

the result. However, particular features of the semiannual oscillation at the stratopause do show a sensitivity to the gravity wave parameterization setting, as was already shown by a simple sensitivity test [*Manzini et al.*, 1997]. Within the lower equatorial stratosphere, neither the CNTRL nor the EXP2 simulations produce a realistic quasi biennial oscillation, although the zonal wind anomaly to the climatological average does show lower frequency variations, a feature common to other general circulation models [*Cariolle et al.*, 1993; *Hamilton et al.*, 1995].

Another remarkable difference between the two simulations is noted in the summer hemispheres, for both January and July. Namely, the easterlies in the upper mesosphere are much stronger (in particularly in January, with differences up to 30-40 m s^{-1}) in the EXP2 than in the CNTRL simulation. The EXP2 summer easterlies are in much better agreement with the CIRA(1986) data.

Figure 8 shows the residual mean stream function (computed following the transformed Eulerian mean formulation [*Andrews et al.*, 1987]) for January and July from the CNTRL and for the EXP2-CNTRL difference. The CNTRL stream function clearly depicts the upwelling at the equator and the single cell circulation in the middle atmosphere, with rising motions in the summer hemisphere and descending motion in the winter hemisphere. Also, a seasonal asymmetry in the circulation is noted, namely, a stronger circulation in January than in July in the stratosphere, in agreement with estimates of the residual circulation from observations [*Rosenlof*, 1995]. For July it is evident that the residual mean circulation is enhanced in EXP2 with respect to CNTRL throughout the middle atmosphere. This enhancement demonstrates that the warming of the polar winter stratosphere and the cooling of the summer upper mesosphere occurring in EXP2 with respect to the CNTRL are of dynamical origin. In January, in the mesosphere the residual mean meridional circulation is also enhanced in EXP2 with respect to the control, while in the stratosphere the EXP2 circulation is actually reduced. The total drag in the stratosphere (the sum of the EP flux divergence from the resolved waves and the total gravity wave tendency) is in fact reduced in the EXP2 experiment in the stratosphere for January.

The total (sum of DSP and orographic) gravity wave tendency from the two experiments is compared in Figure 9, where the January and July zonal mean fields, 10-year ensemble mean, are shown. In both months the total gravity wave tendency does not present dramatic changes in the summer hemisphere (the difference plots however shows that the EXP2 deceleration is larger, except in the subtropical latitude band in the mesosphere). During winter the distribution of the total gravity wave tendency does differ remarkably. In both January and July the total gravity wave tendency in EXP2 is characterized by local deceleration maxima at middle - high latitudes close to 0.1 hPa. Part of the gravity wave momentum flux deposition in the EXP2

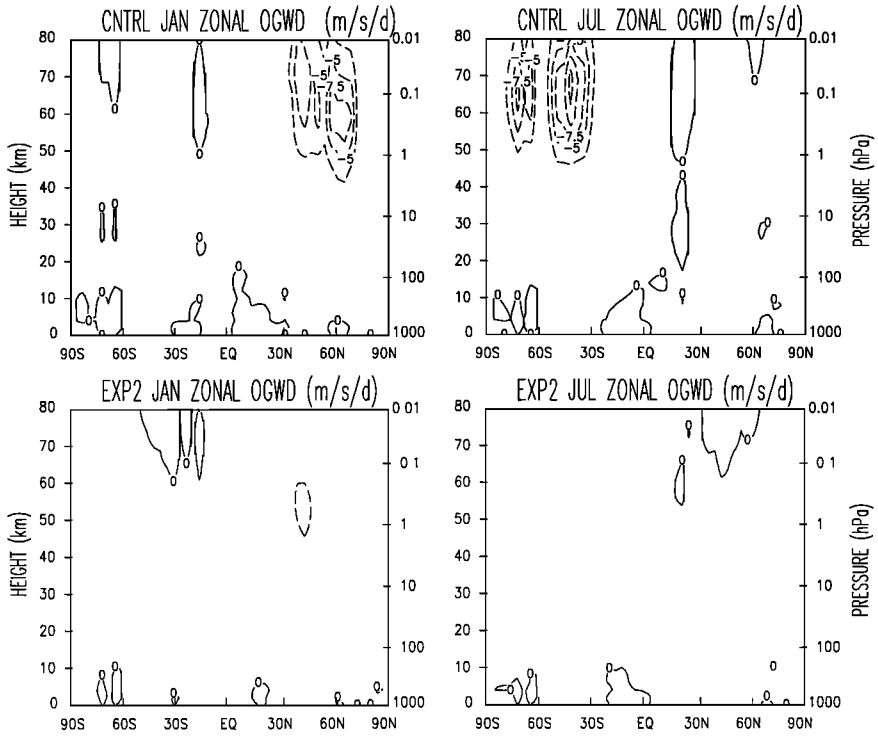

Figure 10. Ensemble mean of the zonal mean of the orographic gravity wave zonal drag from (top) the CNTRL and (bottom) the EXP2 simulations. January is at left, and July is at right. The contour interval is 2.5 m s^{-1} d^{-1}.

integration therefore no longer occurs at the top of the model, but takes place lower down in the middle mesosphere. The appearance of a second drag maximum at lower altitudes is responsible for the large circulation changes shown in Figure 7 and 8 and associated temperature changes shown in Figure 6. The orographic component to the total gravity wave tendency (Figure 10) is substantially reduced in the EXP2, however, because the simulated middle atmosphere winds are substantially smaller in that simulation.

4. Changes in Gravity Waves

In this section the attention is on determining what are the relevant changes in the parameterized gravity wave spectrum of the two experiments that bring about the remarkable changes in the large-scale (resolved) circulation of the middle atmosphere reported above. As was described in section 2, the two experiments are forced by a homogeneous (in space and time) and isotropic spectrum of gravity waves, launched at different heights in the two experiments, namely a pressure level (110 hPa) close to the tropopause in the CNTRL simulation and the surface in EXP2. Possible reasons for the changes in the flow resolved by the general circulation model may therefore include variations associated with how the current parameterization represent the propagation of the gravity waves through the troposphere.

In the control experiment the azimuthally isotropic gravity wave spectrum launched at 110 hPa has a total rms wind speed of 1.75 m s^{-1}, uniform in time and space. It is therefore of interest to evaluate at 110 hPa the total rms wind speed that results from the EXP2 experiment, where the spectrum is launched at the surface.

The total gravity wave rms wind speed for each January and July from the EXP2 simulation is shown in Figure 11. On average the zonal mean gravity wave rms wind speed that results from the EXP2 simulation is smaller in the tropics, about 1 m s^{-1} in the vicinity of the equator, and then increases poleward. In both hemispheres, the rms wind speed poleward increase is larger in summer than in winter. The rms wind speed reaches 2 m s^{-1} at high latitudes in summer, while in winter the rms wind speed is 1.5 m s^{-1}. Given that a rms wind speed of 1.5 m s^{-1} was launched at the surface in EXP2 experiment, a substantial filtering from the tropospheric winds must have occurred in order to balance the rms wind speed increase expected from the decrease of the air density between the surface and 110 hPa. Filtering by the tropospheric winds can also explain the smaller rms wind speed in winter, when the tropospheric winds are stronger. Note also that there appears to be very little interannual variability in the monthly zonal mean rms wind speed, given the narrow cluster of the curves.

Concerning the comparison with the control experiment, it is of interest to note that the EXP2 gravity wave rms wind speed emerging from the troposphere

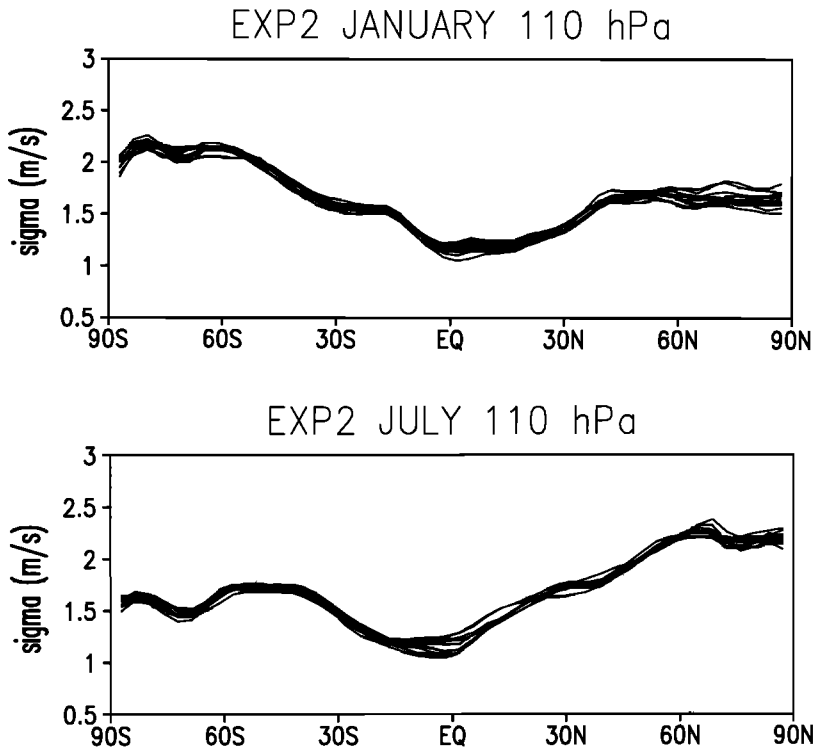

Figure 11. Zonal mean of the total gravity wave rms wind speed from the EXP2 simulation at 110 hPa. Each curve is a monthly mean from the 10-year integration. January is at top, and July is at bottom.

is on average comparable to that used in the control at the launching height. In particular, during winter, when the largest changes in the large scale circulation have been reported, the EXP2 gravity wave rms wind is on average slightly smaller. The warming of the polar stratosphere found in EXP2 appears therefore not to be directly related to the total gravity wave forcing emerging from the troposphere.

From Figure 11 it has already been suggested that the filtering of gravity waves by the tropospheric winds limits the growth of the rms wind with height within the troposphere. In addition, it is expected that only waves that propagate in the direction of the background wind are filtered out, thus producing an anisotropic distribution of the gravity waves at 110 hPa. This differential azimuthal filtering in the EXP2 simulation is shown in Figure 12, where the components of the momentum flux projected in the eastward and westward azimuths are plotted as long- and short-dashed curves, respectively. Also shown, for comparison, is the eastward (or westward, they are identical by contruction) momentum flux (open circles) of the control at 110 hPa, as well as the eastward momentum flux of EXP2 at the surface (solid line).

At 110 hPa, above the location of the tropospheric jets, the eastward momentum flux is strongly reduced with respect to its surface value. In addition, it is also considerably smaller then the value at 110 hPa in the control simulation. In contrast, in the tropics, both the eastward and westward components of the momentum flux are reduced, presumably the result of filtering by strong nonzonal components of the tropospheric flow. At high latitudes, the eastward and westward momentum fluxes are reduced by a similar amount. Therefore their net effect on the background flow averaged over the troposphere should be small.

As may be expected from the previous discussion, in the EXP2 experiment the gravity wave net zonal momentum flux is negative at midlatitudes in the troposphere, as is shown in Figure 13 for the January and July zonal average. In the stratosphere, the net momentum flux remains negative only in the winter hemispheres (because eastward moving gravity waves are removed), while it becomes positive in the summer hemispheres. The easterlies in the summer hemisphere in fact facilitate the dissipation of westward moving gravity waves.

In the control integration the gravity wave momentum flux is assumed to be isotropic at the launching height. Therefore the net flux is zero at 110 hPa. In the stratosphere, the CNTRL zonal net momentum flux at midlatitudes is positive because just above the launching height the westerlies decrease with height, therefore filtering out westward gravity waves with respect to the (relatively large and positive) winds at the launching height. At high latitudes in winter the net momentum flux is negative also in the CNTRL integration. The most remarkable differences between the two experi-

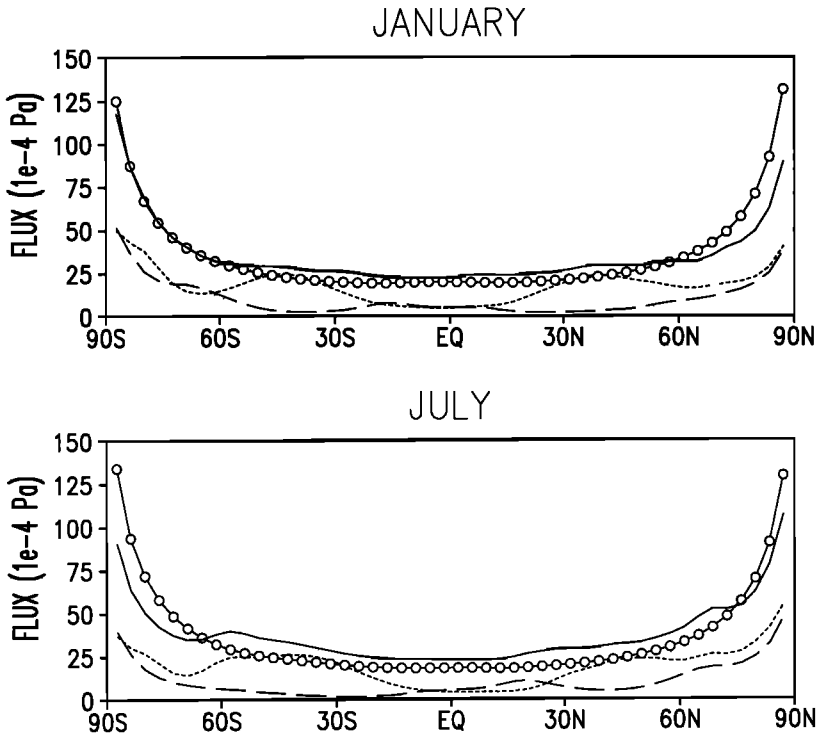

Figure 12. Zonal mean of the components of the eastward (long-dashed line) and westward (short-dashed line) projected momentum flux (10^{-4} Pa) from the EXP2 simulation at 110 hPa. Zonal mean of the components of the eastward projected momentum flux (10^{-4} Pa) from the CNTRL at 110 hPa (open cicles) and from the EXP2 simulation at the surface (solid line). January ensemble mean at top and July ensemble mean at bottom.

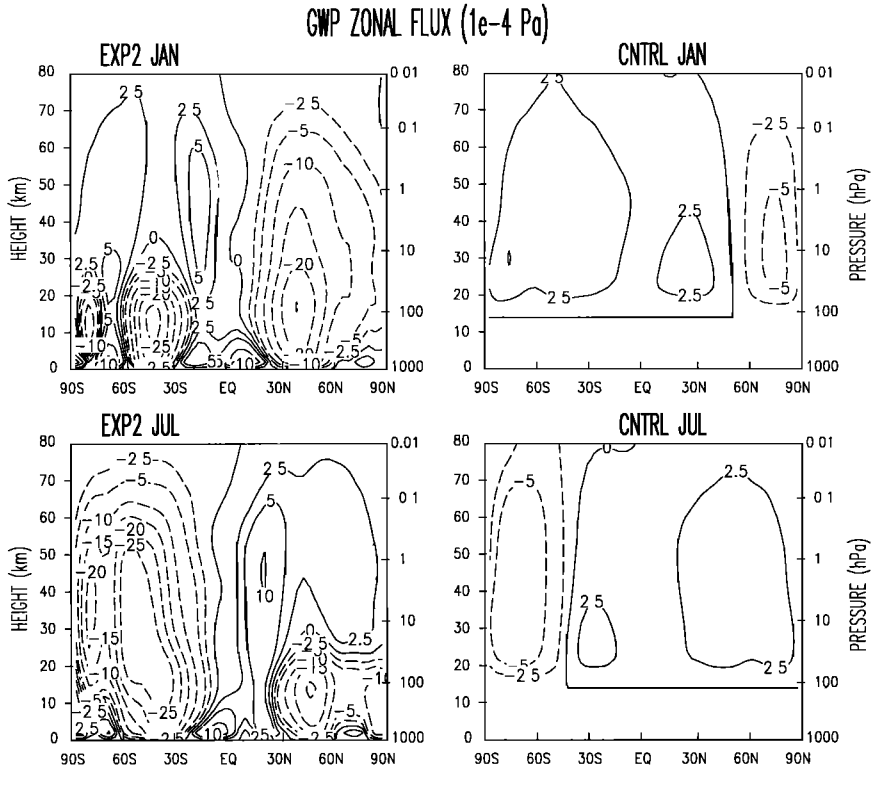

Figure 13. Ensemble mean of the zonal mean of the DSP gravity wave net zonal momentum flux from (right) the CNTRL and (left) the EXP2 simulations. January is at top, and July is at bottom. The contour interval is 2.5x10^{-4} Pa from -5x10^{-4} Pa to 5x10^{-4} Pa, and 5x10^{-4} Pa elsewhere.

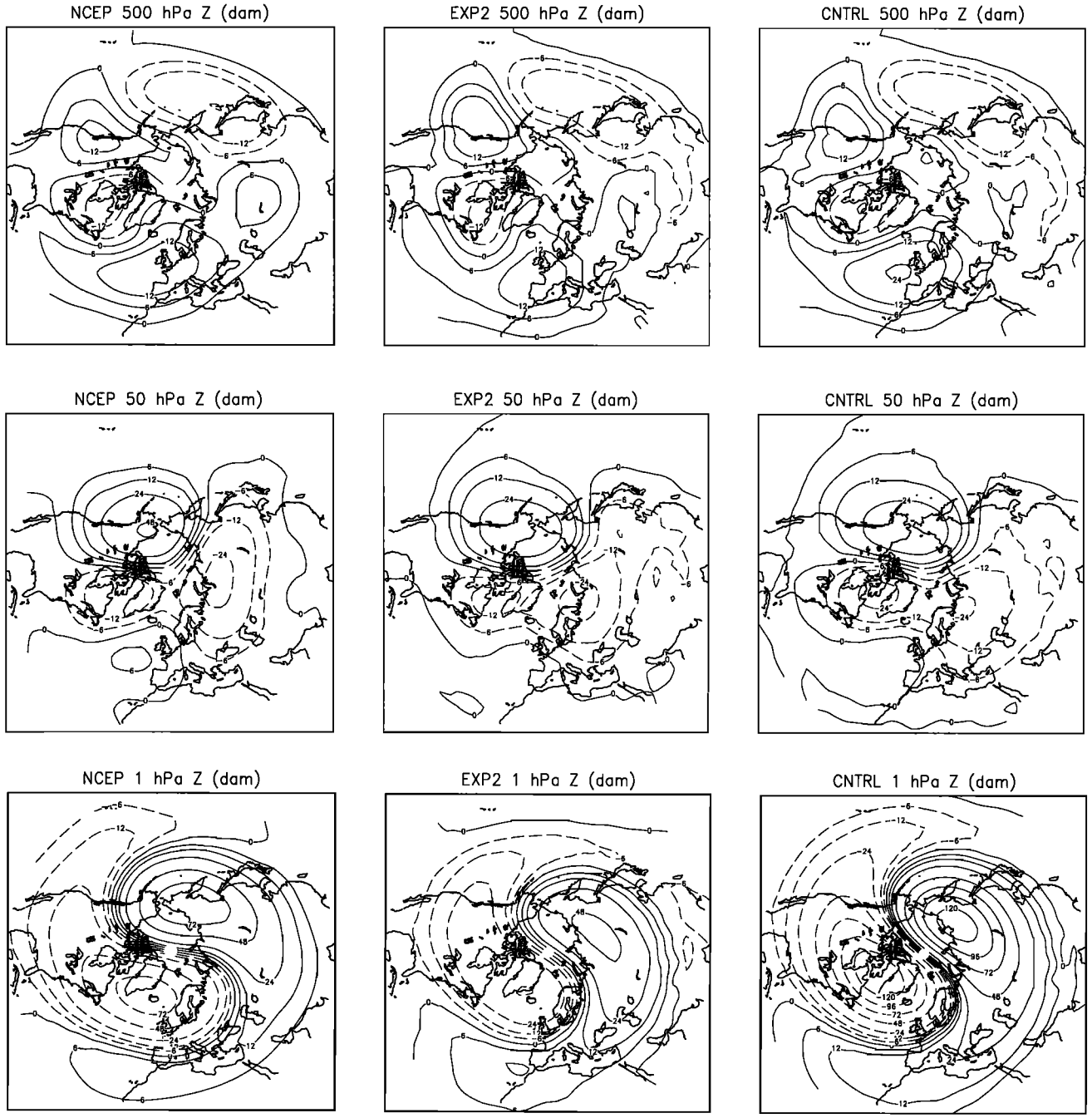

Figure 14. Ensemble mean of the January geopotential height zonal anomaly (left) from the NCEP analysis, (middle) from the EXP2 simulation, and (right) from the CNTRL simulation: polar stereographic map (outer latitude: 20°N) (top) at 500 hPa, (middle) 50 hPa, and (bottom) 1 hPa. Contours are at 0, ±6,±12,±24,±48,±72,±96, ±120 dam.

ments are therefore found in the 20°-50° latitude bands of each hemisphere, where the net momentum flux is of opposite sign in the lower stratosphere. In the southern hemisphere winter at 60°S a difference of about an order of magnitude is also noted between the two experiments. In the winter mesosphere, above the core of the polar night stratospheric jet, where the vertical wind shear is negative, the large negative net momentum flux present in EXP2 may therefore be deposited and cause the strong deceleration of the zonal mean flow shown in the previous section.

5. Changes in Planetary Waves

The stationary geopotential height waves for January are shown in Figure 14, from the NCEP data (15-year averages) and from the two experiments (10-year averages), at selected pressure levels: 500, 50 and 1 hPa.

In the troposphere (500 hPa), the zonal height anomalies are dominated by synoptic scale eddies: Troughs (negative anomaly) over eastern North America and the east Asia - western Pacific sector; and high - pressure systems (positive anomaly) over the North Atlantic - western Europe sector, central Asia, and western North America. Both model versions capture the pattern and strength of the tropospheric stationary eddies. The results from the two experiments are quite similar, only a moderate weakening of the North Atlantic-European height and moderate enhancements of the North Atlantic trough and of the central Asia high are apparent in the EXP2 experiment. The 500 hPa geopotential height difference between the two experiments (not shown) is in fact small, expect over the North Atlantic - western Europe sector where it is reminiscent of the tropospheric - stratospheric mode of variability found in various statistical analysis from observations [*Baldwin et al.,* 1994; *Perlwitz and Graf,* 1995; *Kodera et al.,* 1996]. The North Atlantic - western Europe sector might therefore be the region where the middle atmosphere circulation changes seen in the previous section and related to the strength of the polar night jet could affect the tropospheric circulation. Further analysis of the simulations would be required to evaluate in detail this downward effect, outside the scope of this paper, although of interest.

At lower pressure levels, where the westerlies are stronger, the synoptic scales are filtered out [*Charney and Drazin,* 1961]: at the 50 hPa level the NCEP height anomaly is dominated by a stationary planetary wavenumber 2 and a wavenumber 1 emerges at 1 hPa. The filtering by the westerlies of the synoptic scales is captured by both simulations.

At 50 hPa and at middle latitudes at 1 hPa, there is still good agreement between the simulations and the observations. In contrast, at polar latitudes at 1 hPa, a noticeable difference appears: The positive and negative peaks (over northwestern Asia and Greenland, respectively) of the height anomalies are about a factor of 2 smaller in EXP2 than in the control integration. In comparison to the NCEP stationary waves, it therefore appears that the CNTRL stationary waves are somewhat too strong at 1 hPa at polar latitudes (poleward of 60°N), while the EXP2 waves are too weak. The spacial structure of the simulated waves does not appear to be substantially affected, however, and is also in relatively good agreement with the NCEP wave structure. A substantial reduction of the amplitude of wavenumber 1 and 2 in the upper stratosphere and lower mesosphere at high latitudes is also obtained from the zonal decomposition of the geopotential height and temperature fields (not shown).

Possible reasons for the decrease in the planetary wave amplitude in EXP2 with respect to CNTRL include changes in wave propagation and dissipation due to the reported changes in the zonal mean flow. In this case, the gravity wave parameterization would affect the planetary waves indirectly, though the changes that it induces on the zonal mean flow (Figure 7), and the planetary wave induced mean flow driving would trigger a feedback mechanism that would further reduce the mean flow [*Boville,* 1986]. The momentum flux deposition due to the parameterized gravity waves may have however also a direct effect on the planetary waves, by damping the planetary waves and/or by providing a generation mechanism [*Miyahara et al.,* 1986; *McLandress and McFarlane,* 1993; *Smith,* 1996, 1997]. Evaluating the relative importance of the indirect or direct effect of the gravity waves on the planetary waves is difficult in the context of the simulations being discussed here. This goal would be more conveniently achieved with more idealized experiments in a more simplified setting than that of a general circulation model. At the present stage, only evidence that the DSP gravity wave momentum flux deposition does play a direct role in damping the planetary waves in the EXP2 simulation is shown in Figure 15, where the meridional wind, the DSP gravity wave net meridional momentum flux, and the DSP gravity wave meridional tendency are plotted at 65°N.

The filtering by the tropospheric winds of the gravity waves demonstrated for the zonal mean flow (previous section) that occurs in EXP2 is found to occur also for the zonally varying flow (the meridional flow is show in Figure 15 because of its more pronounced zonal asymmetry). Figure 15 shows in fact that when the meridional tropospheric wind is positive (negative) the net meridional momentum flux is negative (positive). A similar filtering by the stratospheric winds is also found in the control integration (Figure 15, right). However, as in the case of the zonal mean, also the local (i.e., zonally varying) net momentum flux is substantially larger in EXP2 than in CNTRL in the lower stratosphere, thus favoring the dissipation of the planetary waves at a lower altitude in EXP2 than in CNTRL. In the case of the EXP2 experiment, the meridional wind is found therefore to sharply decrease in strength with height in the lower mesosphere (in particular between 60°W and 120°W and around 60°E). In contrast, the CNTRL meridional wind starts to decrease sharply only in the upper mesosphere, where the CNTRL DSP gravity wave tendency is quite large. Note also that above the mid-mesospheric (~0.1 hPa) maxima of the DSP gravity wave deceleration in EXP2, the meridional wind is anticorrelated with the stratospheric meridional wind (at 10 hPa, for instance), in agreement with the observations of *Smith* [1996].

As in the case of the zonal mean (Figure 10), the three-dimensional orographic gravity wave drag is decreased in EXP2 with respect to the control integration. The orographic gravity wave drag can not therefore contribute to an increase in the dissipation of the planetary waves.

The decrease in the strength of the planetary waves in EXP2 in the upper stratosphere and lower mesosphere

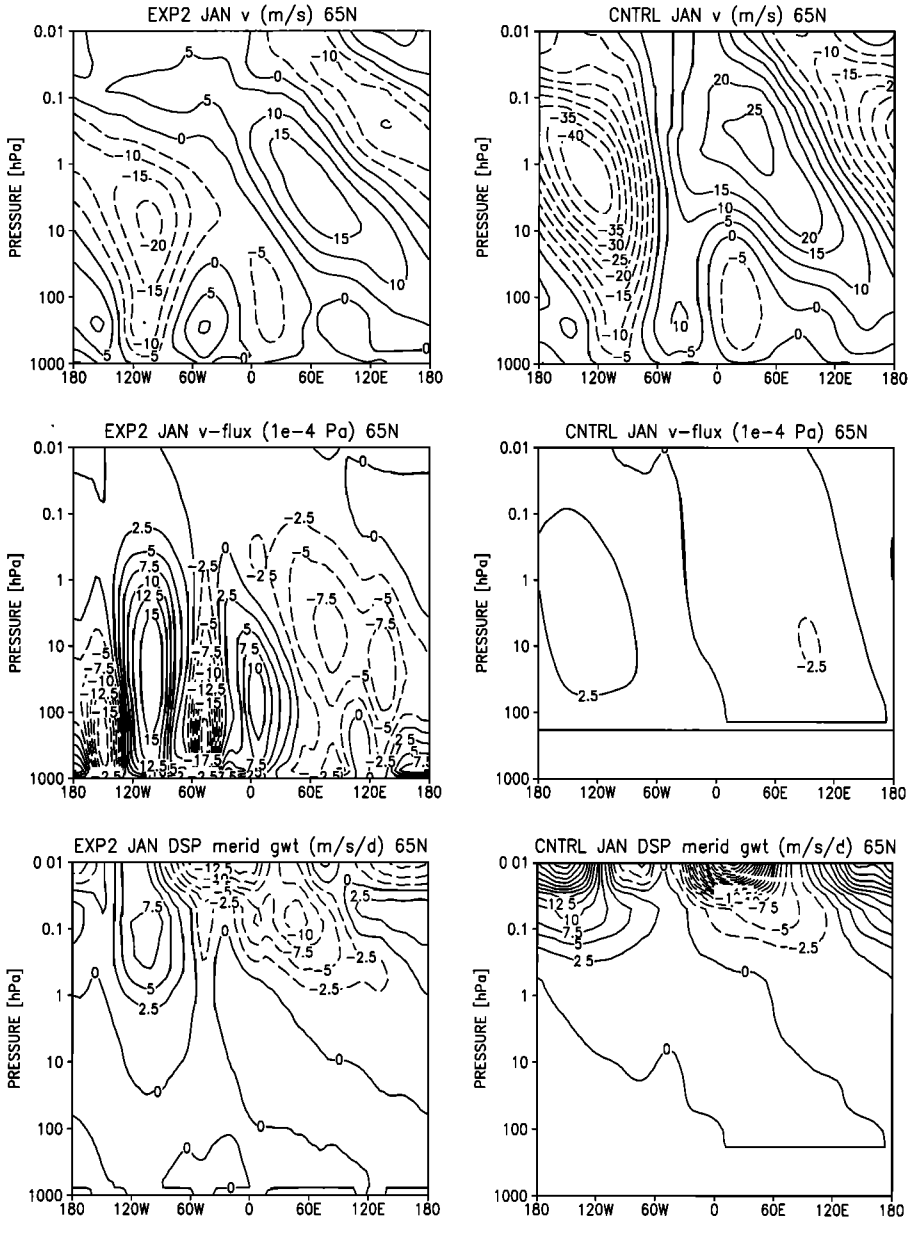

Figure 15. (top) January ensemble mean of the meridional wind, (middle) the DSP gravity wave net meridional momentum flux and (bottom) the DSP gravity wave meridional tendency from the (left) EXP2 and (right) CNTRL simulations: longitude-height section at 65°N. The contour interval for the wind is 5 m s^{-1}. The contour interval for the momentum flux is 2.5x10^{-4} Pa. The contour interval for the tendency is 2.5 m s^{-1} d^{-1}.

at high latitudes is also accompanied by an increase in the Eliassen-Palm (EP) flux convergence (body force per unit mass) in EXP2 with respect to CNTRL (see Figure 16). In the CNTRL integration, Figure 16 shows that the resolved waves exert a negative force on the zonal mean flow throughout most of the winter middle atmosphere. The largest deceleration occurs at mid-latitudes in the lower mesosphere. The EXP2-CNTRL difference indicates that at high latitudes (60°-70°N) in the mesosphere the EP-flux convergence (i.e., deceleration) is enhanced in the EXP2 experiment. In contrast, at middle latitude the difference is positive, i.e., the EP-flux convergence is reduced in the EXP2 experiment. A larger EP-flux convergence at high latitudes, where the planetary waves are most reduced, is consistent with the suggestion that the EXP2 planetary waves are dissipated in the lower mesosphere by the DSP gravity wave parameterization (although planetary wave - mean flow interactions and forcing by the orographic gravity wave drag at middle latitudes cannot be ruled out). Figure

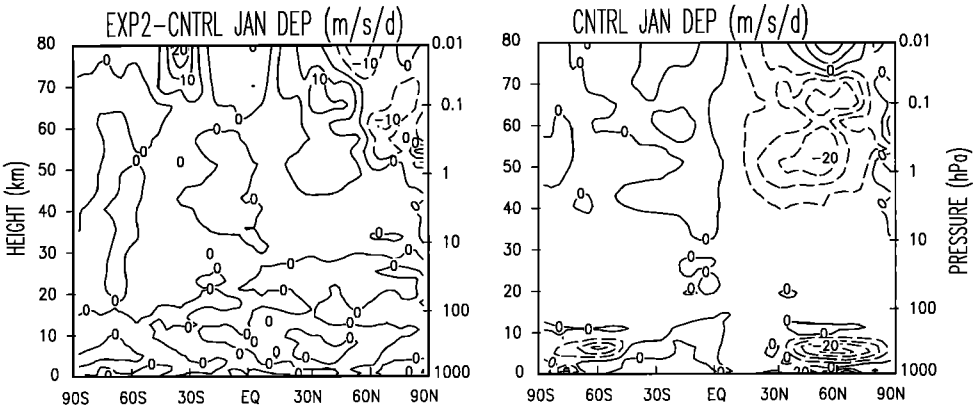

Figure 16. (right) January ensemble mean of the EP flux divergence from the CNTRL simulation and (left) difference between the EXP2 and CNTRL simulations, EXP2-CNTRL, of the January ensemble mean of the EP flux divergence. The contour interval is 5 m s^{-1} d^{-1}.

16 also shows that differences in the EP divergence in the troposphere are relatively small (less then 5 m s^{-1} d^{-1}).

6. Summary and Conclusions

The sensitivity of the long-term response of the middle atmosphere circulation simulated using a general circulation model to changes in the source spectrum of a gravity wave parameterization has been investigated by performing two 10-year integrations. The general circulation model used is the MA/ECHAM4 model (surface to 80 km) and the parameterization of the momentum flux deposition due to a continuous gravity wave spectrum is based on the Doppler spread formulation of *Hines* [1997a, b]. In addition to the Doppler spread parameterization, the general circulation model includes a modified version of the *McFarlane* [1987] orographic gravity wave drag parameterization. Currently, the two gravity wave parameterizations are uncoupled.

The first 10-year integration performed with the MA ECHAM4 model, CNTRL, employs for the DSP gravity wave spectrum a launching height at the 110 hPa pressure level and a gravity wave rms wind speed there of 1.75 m s^{-1}. In the second 10-year integration, EXP2, the source spectrum is instead launched at the surface with a gravity wave rms wind speed of 1.5 m s^{-1}. The present work focus on the long time average behavior, the analysis of the time variability (from interannual to daily scales) of the model results is progress.

The simulation of the lower stratosphere of the CNTRL experiment presents several realistic features: a small zonal mean temperature bias (less than 5 K); the strength, structure and seasonal evolution of the zonal wind in agreement with observations; and in the northern hemisphere winter realistic stationary eddies. In contrast, in the upper stratosphere and mesosphere the simulation of the southern winter stratosphere is affected by a substantial cold temperature bias and the northern winter stationary eddies are somewhat too strong at polar latitudes. These model deficiencies have been found to be sensitive to the gravity wave forcing.

The effects of varying the source spectrum can be summarized as follows: (1) With respect to the control experiment, the experiment with the surface as the launching height (EXP2) presents a remarkable improvement in the simulation of the long-term zonal mean circulation of the polar stratosphere during the southern winter and spring. The polar cold temperature bias is virtually eliminated in EXP2. (2) Strong easterlies in the subtropical mesosphere characterize EXP2 in summer, again an improvement. (3) In the EXP2 experiment, the stationary waves are substantially reduced in the northern winter upper stratosphere and mesosphere. This reduction in the strength of the planetary waves might be excessive, given that the model bias changes from too strong (CNTRL) to too weak (EXP2) planetary waves. (4) In the northern hemisphere winter, the zonal mean circulation is too much reduced in the EXP2 simulation.

Changes in planetary waves that occur in the southern hemisphere between the two simulations are also remarkable but are not shown in this work. A preliminary analysis indicates that in the southern hemisphere there is a difference in the relative role played by the largest planetary waves in the two experiments. In July, for instance, the CNTRL height field appears to be dominated by a wavenumber 2 pattern (in contrast with observations), while wavenumber 1 dominates in EXP2 (in agreement with observations).

Diagnostics of the parameterized gravity waves indicate that the differences in the zonal mean state as well as the differences in the northern hemisphere planetary waves are related to the gravity wave net mo-

mentum flux emerging from the troposphere. In the EXP2 experiment the gravity wave net zonal momentum flux emerging from the troposphere is negative at middle and high latitudes throughout the year. In contrast, in the experiment with launching height at 110 hPa, the gravity wave net momentum flux is zero by construction at the launching height. In the EXP2 experiment the negative net zonal momentum flux above the troposphere facilitates the deceleration of the westerlies in the mesosphere, above the core of the winter stratospheric eastward jet. In contrast, the negative net zonal momentum flux limits the upper mesospheric deceleration of the easterlies in summer. The strong deceleration of the westerlies in the lower mesosphere that occurs in the EXP2 simulation therefore induces a residual mean meridional circulation that causes the reported substantial warming (with respect to the control) of the southern hemisphere polar winter stratosphere. In the control experiment the deceleration associated with the DSP tendency is instead confined to the upper mesosphere, close to the model top. The descent of the DSP deceleration also appears to be one reason for the reduction in the northern winter planetary wave amplitudes in the upper stratosphere and lower mesosphere found in EXP2. In addition, in the northern hemisphere there seems to be some compensation among the various forms of drags (from the DSP, the orographic gravity wave drag and from the resolved waves). This compensation might be the reason why the temperature and circulation changes in the northern hemisphere winter, although noticeable, are not as remarkable as those in the southern hemisphere winter.

Concerning the problem of how to specify the source spectrum of a gravity wave parameterization, the present work has emphasized the importance of the filtering of the gravity waves by the tropospheric background winds, or, in other words, it has drawn attention to the limitation of the isotropic assumption for a source spectrum launched at a level close to the tropopause. It is noted that reports from observations tend to indicate a negative momentum flux transported by gravity waves in the lower stratosphere at middle and high latitudes (see, for instance, *Vincent et al.* [1997]), with respect to the background flow.

The present work has also shown that within a realistic range of the parameter setting of the gravity wave parameterization employed, it is possible to virtually eliminate the winter polar temperature bias in the general circulation model. However, a specification of the source spectrum that allows for seasonal and geographical variability is clearly required for a successful simulation of the seasonal cycle of the middle atmosphere circulation.

This work has also raised questions concerning the interactions between the resolved and parameterized waves in a general circulation model. This topic as only been touched in the present work, by presenting evidence of damping of planetary waves by the parameterized gravity waves in the lower mesosphere.

Acknowledgments. The authors would like to thank L. Bengtsson for support and encouragements and the official reviewers for helpful and constructive comments that improved the manuscript. We are grateful to M. Giorgetta for providing the code for the transformed Eulerian mean diagnostics, and to U. Schlese and colleagues at DKRZ and MPI for technical assistance. E. Manzini was partly supported by the project "Impact of Gravity Waves on Climate' by the European Commision Environment and Climate Research Programme (Contract: ENV4-CT97-0486, Climate and Natural Hazards).

References

Allen, S. J., and R. A. Vincent, Gravity wave activity in the lower atmosphere: Seasonal and latitudinal variations, *J. Geophys. Res., 100*, 1327-1350, 1995.

Andrews, D. G., J. R. Holton, and C. B. Leovy, *Middle Atmospheric Dynamics,* 489 pp., Academic, San Diego, Calif., 1987.

Baldwin, M. P., X. Cheng, and T. J. Dunkerton, Observed correlations between winter mean tropospheric and stratospheric circulation anomalies, *Geophys. Res. Lett.*, it 21, 1141-1144, 1994.

Boville, B. A., Wave mean flow interactions in a general circulation model of the troposphere and stratosphere, *J. Atmos. Sci., 43*, 1711-1725, 1986.

Boville, B. A., Middle atmosphere version of the CCM2 (MACCM2): Annual cycle and interannual variability, *J. Geophys. Res., 100*, 9017-9039, 1995.

Brinkop, S., and E. Roeckner, Sensitivity of a general circulation model to parameterizations of cloud-turbulence interactions in the atmospheric boundary layer, *Tellus, Ser. A, 47*, 197-220, 1995.

Brühl, C., Atmospheric effects of stratospheric aircraft. Models and Measurements Workshop, edited by M. Prather and E. Remsberg. *NASA Ref. Publ., 1292 II*, 1993.

Cariolle, D., M. Amodei, M. Deque, J.-F. Mahfouf, P. Simon, and H. Teyssedre, A quasi biennial oscillation signal in general circulation model simulations, *Science, 261*, 1313-1316, 1993.

Charney, J. G., and P. G. Drazin, Propagation of planetary scale disturbances from the lower into the upper atmosphere, *J. Geophys. Res., 66*, 83-109, 1961.

Fels, S. B., Radiative-dynamical interactions in the middle atmosphere, *Adv. Geophys., 28A*, 277-300, 1985.

Fleming, E. L., S. Chandra, J. J. Barnett, and M. Corney, Zonal mean temperature, pressure, zonal wind and geopotential height as functions of latitude, *Adv. Space Res., 10, N12*, 1211-1259, 1990.

Fleming, E. L., S. Chandra, M. D. Burrage, W. R. Skinner, P. B. Hays, B. H. Solheim, and G. G. Shepherd, Climatological mean wind observations from the UARS high-resolution Doppler imager and wind imaging interferometer: Comparison with current reference models, *J. Geophys. Res., 101*, 10455-10473, 1996.

Fouquart, Y. and B. Bonnel, Computations of solar heating of the Earth's atmosphere: A new parametrization. *Beitr. Phys. Atmos., 53*, 35-62, 1980.

Fritts, D. C., and W. Lu, Spectral estimates of gravity wave energy and momentum fluxes, II, Parameterization of wave forcing and variability, *J. Atmos. Sci., 50*, 3695-3713, 1993.

Fritts, D. C., and G. D. Nastrom, Sources of mesoscale variability of gravity waves, II, Frontal, convective and jet stream excitation, *J. Atmos. Sci., 49*, 111-127, 1992.

Garcia, R. R., and B. A. Boville, "Downward control" of the mean meridional circulation and temperature distribution of the polar winter stratosphere, *J. Atmos. Sci., 51*, 2238-2245, 1994.

Gates, W. L., AMIP: The Atmospheric Model Intercomparison Project, *Bull. Am. Meteorol. Soc., 73*, 1962-1970, 1992.

Giorgetta, M., and M., Wild, The water vapour continuum and its representation in ECHAM4, *MPI Rep. 162*, 32 pp., Max-Planck-Inst. für Meteorol., Hamburg, Germany, 1995.

Hamilton, K., R. J. Wilson, J. D. Mahlman, and L. J. Umscheid, Climatology of the SKYHI troposphere stratosphere mesosphere general circulation model, *J. Atmos. Sci., 52*, 5-43, 1995.

Haynes, P. H., C. J. Marks, M. E. McIntyre, T. G. Shepherd, and K. P. Shine, On the "downward control" of extratropical diabatic circulations by eddy-induced mean zonal forces, *J. Atmos. Sci., 48*, 651-678, 1991.

Hines, C. O., Doppler spread parameterization of gravity wave momentum deposition in the middle atmosphere, 1, Basic formulation, *J. Atmos. Solar Terr. Phys., 59*, 371-386, 1997a.

Hines, C. O., Doppler spread parameterization of gravity wave momentum deposition in the middle atmosphere, 2, Broad and quasi monochromatic spectra and implementation, *J. Atmos. Solar Terr. Phys., 59*, 387-400, 1997b.

Hitchman, M. H., J. C. Gille, C. D. Rodgers, and G. Brasseur, The separated polar winter stratopause: A gravity wave driven climatological feature, *J. Atoms. Sci., 46*, 410-422, 1989.

Holton, J. R., P. H. Haynes, M. E. McIntyre, A. R. Douglass, R. B. Rood, and L. Pfister, Stratosphere-troposphere exchange, *Rev. Geophys., 33*, 403-439, 1995.

Kodera, K., M. Chiba, H. Koide, A. Kitoh, and Y. Nikaidou, Interannual variability of the winter stratosphere and troposphere in the northern hemisphere, *J. Meteorol. Soc. Jpn., 74*, 365-382, 1996.

Lawrence, B. N., and W. J. Randel, Variability in the mesosphere observed by the Nimbus 6 pressure modulator radiometer, *J. Geophys. Res., 101*, 23,475-23,489, 1996.

Lübken, F.-J. and U. von Zahn, Thermal structure of the mesopause region at polar latitudes, *J. Geophys. Res., 96*, 20,841-20,857, 1991.

Manzini, E., and L. Bengtsson, Stratospheric climate and variability from a general circulation model and observations, *Clim. Dyn., 12*, 615-639, 1996.

Manzini, E., N. A. McFarlane, and C. McLandress, Impact of the Doppler spread parameterization on the simulation of the middle atmosphere circulation using the MA ECHAM4 general circulation model, *J. Geophys. Res., 102*, 25,751-25,762, 1997.

McFarlane, N.A., The effect of orographically exited gravity wave drag on the general circulation of the lower stratosphere and troposphere, *J. Atmos. Sci., 44*, 1775-1800, 1987.

McIntyre, M. E., Atmospheric dynamics: Some fundamentals, with observational implications, in *The Use of EOS for Studies of Atmospheric Physics*, edited by J.C. Gille and G. Visconti, *Proc. Int. Sch. Phys. E. Fermi*, 313-386, 1992.

McLandress, C., and N. A. McFarlane, Interactions between orographic gravity wave drag and forced stationary planetary waves in the winter northern hemisphere middle atmosphere, *J. Atmos. Sci., 50*, 1966-1990, 1993.

Medvedev, A. S., and G. P. Klaassen, Vertical evolution of gravity wave spectra and the parameterization of associated wave drag, *J. Geophys. Res., 100*, 25,841-25,853, 1995.

Miyahara, S., Y. Hayashi and J.D. Mahlman, Interactions between gravity waves and planetary scale flow simulated by the GFDL SKYHI general circulation model, *J. Atmos. Sci., 43*, 1844-1861, 1986.

Morcrette, J. J., Radiation and cloud radiative properties in the European Centre for Medium-Range Weather Forecasts forecasting system, *J. Geophys. Res., 96*, 9121-9132, 1991.

Nordeng, T. E., Extended versions of the convective parameterization scheme at ECMWF and their impact on the mean and transient activity of the model in the tropics, *ECMWF Tech. Memo. 206*, 41 pp., Eur. Cent. for Medium-Range Weather Forecasts, Reading, England, 1994.

Perlwitz, J., and H. F. Graf, The statistical connection between tropospheric and stratospheric circulation of the northern hemisphere winter, *J. Clim., 8*, 2281-2295, 1995.

Randel, W. J., Global atmospheric circulation statistic, 1000-1 mb, *Tech. Rep. TN-366+STR*, Nat. Cent. Atmos. Res., Boulder, Colo., 1992.

Roeckner, E., Parameterization of cloud radiative properties in the ECHAM4 model, in *Cloud Microphysics Parameterizations in Global Atmospheric Circulation Models, WRCP Rep. 90, WMO/TD-No.713*, 105-116, World Clim. Res. Program, Geneva, 1995.

Roeckner, E., K. Arpe, L. Bengtsson, M. Christoph, M. Claussen, L. Dümenil, M. Esch, M. Giorgetta, U. Schlese, and U. Schulzweida, The atmospheric general circulation model ECHAM4: Model description and simulation of present-day climate, *MPI Rep. 218*, 90 pp., Max-Planck-Inst. für Meteorol., Hamburg, Germany, 1996a.

Roeckner, E., J. M. Oberuber, A. Bacher, M. Christoph, and I. Kirchner, ENSO variability and atmospheric response in a global coupled atmosphere-ocean GCM, *Clim. Dyn., 12*, 734-754, 1996b.

Roeckner, E., M. Rieland, and E. Keup, Modelling of cloud and radiation in the ECHAM model, in *Cloud, Radiative Transfer and the Hydrological Cycle, ECMWF/WCRP Proc.*, 199-222, Eur. Cent. for Medium-Range eather Forecasts, Reading, England, 1991.

Rosenlof, K. H., Seasonal cycle of the residual mean meridional circulation in the stratosphere, *J. Geophys. Res., 100*, 5173-5191, 1995.

Shine, K. P., The middle atmosphere in the absence of dynamical heat fluxes, *Q. J. R. Meteorol. Soc., 113*, 603-633, 1987.

Smith, A. K., Longitudinal variations in mesospheric winds: Evidence for gravity wave filtering by planetary waves, *J. Atmos. Sci., 53*, 1156-1173, 1996.

Smith, A.K., Stationary planetary waves in upper mesospheric winds, *J. Atmos. Sci., 54*, 2129-2145, 1997.

Sundqvist, H., A parameterization scheme for non-convective condensation including prediction of cloud water content, *Q. J. R. Meteorol. Soc., 104*, 677-690, 1978.

Tiedtke, M., A comprehensive mass flux scheme for cumulus parameterization in large-scale models, *Mon. Weather Rev., 117*, 1779-1800, 1989.

Williamson, D. L. and P. J. Rasch, Water vapour transport in the NCAR CCM2, *Tellus, Ser. A, 46*, 34-51, 1994.

Vincent, R.A., S.J. Allen, and S.D. Eckermann, Gravity wave parameters in the lower stratosphere, in *Gravity Wave Processes and Their Parameterization in Global Climate Models*, edited by K. Hamilton, *NATO ASI Ser. I, 50*, 7-25, 1997.

E. Manzini, Max Planck Institut für Meteorologie, Bundesstrasse 55, 20146 Hamburg, Germany. (e-mail: manzini@dkrz.de)

N. A. McFarlane, Canadian Centre for Climate Modelling and Analysis, Atmospheric Environment Service, University of Victoria, P.O. Box 1700, Victoria, B. C. V8W 2Y2, Canada. (email: Norm.McFarlane@ec.gc.ca)

(Received February 3, 1998; revised June 17, 1998; accepted July 7, 1998.)